American Mineralogist, Volume 88, pages 1104–1114, 2003

Infrared and TEM characterization of amphiboles synthesized near the tremolite-pargasite join in the ternary system tremolite-pargasite-cummingtonite

DAVID M. JENKINS,[1,*] KRASSIMIR N. BOZHILOV,[2] AND KIYOTAKA ISHIDA[3]

[1]Department of Geological Sciences and Environmental Studies, Binghamton University, Binghamton, New York 13902-6000, U.S.A.
[2]Central Facility for Advanced Microscopy and Microanalysis, Institute of Geophysics and Planetary Physics, University of California, Riverside, California 92521, U.S.A.
[3]Department of Evolution of the Earth and the Environment, Graduate School of Social and Cultural Studies, Kyushu University, 4-2-1 Ropponmatsu, Chuo-ku, Fukuoka 810-8560, Japan

ABSTRACT

High-resolution transmission-electron microscopy (HRTEM) and infrared spectroscopy (FTIR) analyses have been done on amphiboles near the join tremolite [$Ca_2Mg_5Si_8O_{22}(OH)_2$ = TR]-pargasite [$NaCa_2Mg_4Al_3Si_6O_{22}(OH)_2$ = PG] in the ternary system tremolite-pargasite-cummingtonite [$Mg_7Si_8O_{22}(OH)_2$ = MC] that were synthesized previously by Sharma and Jenkins (1999). Representative samples across the join were examined in detail by HRTEM to document the presence and concentration of chain multiplicity defects (CMFs). There was relatively little change in the defect density with composition, with the tremolitic sample (TREM 23-13) having the highest defect concentration (6%) and the more PG-rich samples having slightly lower CMF concentrations (4–5%). CMFs with multiplicities of 1, 3, 4, 5, and 6 were observed, usually as isolated chains, with the most common being triple-chain slabs. Correction of the bulk composition of the tremolitic amphibole for the presence of these Mg-rich, wide-chain defects reduces the MC content from an apparent value of 8.5 to 4–7.5 mol% MC, depending on which composition is used for the triple-chain defect. The entire amphibole join was examined by FTIR spectroscopy in the OH-stretching region (3000–3800 cm^{-1}) for the purpose of determining the presence of short-range order. A total of 10 component bands were fitted to the spectra across the join. These bands were assigned to specific cation configurations on the basis of earlier studies of the FTIR spectra of chemically simplified amphibole joins pertinent to this study. The extent of short-range order was qualitatively determined by comparing the observed intensities for groups of related bands, corrected for differences in their molar absorptivities, to their calculated intensities based on random-mixing probabilities. From this exercise, it is observed that the intensities of sodic amphibole configurations are consistently high, tremolite is lowest near the middle of the join, and aluminous amphibole configurations cross over from being higher (at low Al contents) to being lower (at high Al contents) than expected near the middle of the join. These differences between observed and predicted band intensities may reflect the presence of deviations in the thermodynamic activities of amphibole components from those predicted on the basis of random-mixing models.

INTRODUCTION

There has been considerable effort in the past 10 years to document and characterize short-range ordering of cations in amphiboles by such techniques as nuclear-magnetic resonance (NMR) spectroscopy (e.g., Welch et al. 1994; Jenkins et al. 1997; Hawthorne et al. 2000) and Fourier-transform infrared (FTIR) spectroscopy (e.g., Della Ventura et al. 1999; Robert et al. 2000; Melzer et al. 2000; Fialips-Guédon et al. 2000; Della Ventura et al. 2001). This information is necessary to understand the extent of cation mixing that occurs within the amphibole structure, which in turn strongly influences the bulk entropy of the mineral as well as the thermodynamic activities of amphibole components in amphibole solid solutions. Because of the sensitivity of the stretching vibration of the OH anion at the O3 site to the three nearest-neighbor octahedral cations (at the two M1 and one M3 sites) and the relative simplicity of the technique, short-range ordering deduced from FTIR analysis of natural and synthetic amphiboles has been investigated extensively in recent years. These studies complement the long-range cation-ordering information obtained through X-ray and neutron-diffraction studies.

In this study, we present FTIR spectra from samples synthesized near the tremolite [$Ca_2Mg_5Si_8O_{22}(OH)_2$ = TR]-pargasite [$NaCa_2Mg_4Al_3Si_6O_{22}(OH)_2$ = PG] join in the system tremolite-pargasite-cummingtonite [$Mg_7Si_8O_{22}(OH)_2$ = MC] reported earlier by Sharma and Jenkins (1999). This join includes substitution of Al at both octahedral and tetrahedral sites as the Tschermak substitution ($^{VI}Al + {}^{IV}Al = {}^{VI}Mg + {}^{IV}Si$) and substitution of Na at the A site via the edenite substitution ($^{IV}Al + Na = {}^{IV}Si + \square$), which, taken together, may be called the pargasite substitution. Even without the presence of Fe, the FTIR spectra in the OH-stretching region become fairly complex near the middle of the join; however, we can take advantage of the earlier work that has been done on interpreting the FTIR spectra of amphiboles formed along the richterite-pargasite join (Della Ventura et al. 1999) and along the tremolite-

* E-mail: dmjenks@binghamton.edu

aluminotschermakite join (Hawthorne et al. 2000) to help interpret the spectra in terms of key short-range cation configurations.

Another issue that has received considerable attention in recent years is the role that chain-width defects or chain-multiplicity faults (CMFs) play in controlling the chemical composition and bulk thermochemical properties of amphiboles, particularly the presence of either narrow (single-chain) or wider (triple-chain, quadruple-chain, etc.) defects within an otherwise uniformly ordered double-chain silicate (e.g., Ahn et al. 1991; Maresch et al. 1994; Zimmerman et al. 1996). Although there has been some study of the influence of such factors as temperature, fluid pressure, and mineral precursor (i.e., crystalline minerals vs. amorphous oxides vs. gels) in controlling the types or abundances of CMFs within tremolitic amphiboles (Ahn et al. 1991; Maresch et al. 1994; Bozhilov 1997), there is very little information on the control of bulk composition for calcic amphiboles. We report here the results of high-resolution transmission electron microscopy (HRTEM) analysis of some of the same amphibole samples investigated by FTIR spectroscopy. This affords an opportunity to determine (1) how much the chemical composition of these amphiboles is influenced by wide-chain (and presumably Mg-rich) CMFs, and (2) what, if any, dependency the concentration of defects has on bulk composition along this join.

Materials and Methods

Samples

The samples analyzed in this study are synthetic amphiboles formed in the highest-yield experiments of Sharma and Jenkins (1999). In brief, the samples were made from mixtures of reagent-grade oxides and carbonates and treated hydrothermally for durations of 188–879 h in internally heated gas vessels. The nominal bulk compositions of the amphiboles, the pressure and temperature conditions of synthesis, and the observed compositions of the amphiboles (electron microprobe) are summarized in Table 1. The minimum yield of amphibole is for TREM 23-13 (94 wt% amphibole, trace clinopyroxene and quartz); the remaining samples contained 98–100 wt% amphibole with only traces of clinopyroxene and plagioclase. It should be noted that PARG 19-11 (with about 80 mol% of the PG component) has as much Na as end-member pargasite. This Na enrichment was discussed by Sharma and Jenkins (1999) and correlates with an unusually large cell volume and difficulty in making an amphibole at this composition *without* the use of an NaOH-bearing solution.

TEM Analysis

Transmission electron microscopy (TEM) was done at the Central Facility for Advanced Microscopy and Microanalysis of the University of California at Riverside with an FEI-Philips CM300 microscope operating at 300 kV accelerating voltage, equipped with a LaB_6 electron gun, twin objective lens, CompuStage—eucentric side-entry goniometer allowing a high degree of tilt (±70°), low-background double-tilt specimen holder, Gatan anti-contamination device, and an EDAX energy-dispersive spectrometer (EDS).

Samples were prepared by dispersing the crystal aggregates without grinding in distilled water, ultrasonically agitating them, and depositing a drop of the resulting suspension onto Cu grids coated with a thin (5 nm thickness) holey carbon support film. Selected-area electron-diffraction (SAED) patterns and high-resolution (HRTEM) images were obtained for about 15 crystals from each sample. The HRTEM images were obtained with a 50 μm diameter condenser aperture, an effective objective-aperture radius of 0.86 nm^{-1}, spherical aberration (C_s) of 2.00 mm, at defocus values of –60 to –160 nm, and a beam convergence angle of 0.8 mrad. Images were recorded digitally using a Gatan 794 MultiScan CCD camera and DigitalMicrograph 2.5 software running on a Macintosh Power PC 8100/100 computer. HRTEM image interpretation is based on comparison with published data and image simulation done on a Macintosh Power PC G3/333 computer using the MacTempas software.

Selected crystals were imaged with the electron beam perpendicular to the **b*** axis allowing determination of chain-multiplicity fault type and abundance. The CMF abundance was characterized using the $A'(i)$ value as introduced by Ahn et al. (1991) following Maresch and Czank (1988), where $A'(i)$ is the ratio of the chains with a particular multiplicity (i) expressed as the number of silica-tetrahedral chains sharing common corners parallel to **b*** vs. the total number of tetrahedral chains in the crystal. The $A'(1)$, $A'(2)$, and $A'(3)$ values were determined accurately; CFMs with multiplicity larger than three are summarized as one $A'(n)$ value, primarily because of the very low occurrence of such defects.

The compositions of all crystals studied by HRTEM were determined quantitatively by EDS analyses using experimentally determined k-factors and following the procedure of Bozhilov et al. (1999).

FTIR Instrumentation

Infrared spectra were recorded (at Kyushu University) in the range of 3800–3000 cm^{-1} with a JASCO FTIR-620 spectrometer equipped with a DLATGS detector and a KBr beam splitter. A total of 128 scans per sample were measured in an evacuated sample chamber at a nominal resolution of 1.0 cm^{-1}. Samples were prepared for infrared spectroscopy by combining about 200 mg of KBr with 1.5–3.0 mg of fine-grained amphibole and pressing the mixture into 10 mm diameter disks.

Individual bands were fitted to the absorption spectra as follows. First, the background at the frequencies of the bands was modeled by a straight-line tangent to the background well beyond the range of the peaks being fitted. Second, initial estimates of the major band positions and intensities were entered manually based on visual inspection of the pattern. Third, refinement of the initial estimates of peak position, intensity, and full width at half maximum (FWHM) for any given band was carried out using the program ProFit 1.0c. Bands were further adjusted manually as needed and the whole process repeated until an acceptable overall agreement index ($R_{min} \leq 0.3\%$) was obtained. The guiding principle for fitting the spectra was to use the smallest number of bands necessary. Symmetric pseudo-Voigt peak profiles with 50% Gaussian component were used for all bands except the broad, highest-wavenumber band (A) of PARG 11-7, which was better modeled as being 100% Gaussian, and the dominant band (C) of TREM 23-13, which was better modeled with only 25% Gaussian component (i.e., strongly Lorentzian in shape). Once the pseudo-Voigt profile-mixing parameter was determined for a band, this same value was used for all spectra. The band widths, as defined by the full-width at half maximum (FWHM) parameter, were also held constant for a given band for all of the spectra.

Results

HRTEM Analyses

Figure 1 shows representative TEM images of amphiboles from samples TREM 23-13 (0 mol% PG), PARG 21-2 (38 mol%

Table 1. Nominal bulk compositions, synthesis conditions, and observed compositions (electron microprobe analyses) of amphiboles investigated in this study arranged in order of increasing pargasite (PG) component

Code	Nominal composition	Components (mol%)	T(°C)	P(kbar)	t(h)	Observed composition (microprobe)
TREM 23-13	$Ca_{1.80}Mg_{5.20}Si_{8.00}O_{22}(OH)_2$	$PG_0TR_{90}MC_{10}$	801	4.52	458	$Ca_{1.82}Mg_{5.17}Si_{8.00}O_{22}(OH)_2$
PARG 18-3	$Na_{0.195}Ca_{1.83}Mg_{4.975}Al_{0.585}Si_{7.61}O_{22}(OH)_2$	$PG_{19.5}TR_{72}MC_{8.5}$	802	4.00	768	$Na_{0.14}Ca_{1.86}Mg_{4.95}Al_{0.52}Si_{7.67}O_{22}(OH)_2$
PARG 21-2	$Na_{0.38}Ca_{1.78}Mg_{4.84}Al_{1.14}Si_{7.24}O_{22}(OH)_2$	$PG_{38}TR_{51}MC_{11}$	795	4.00	264	$Na_{0.43}Ca_{1.67}Mg_{4.89}Al_{1.23}Si_{7.19}O_{22}(OH)_2$
PARG 20-2	$Na_{0.57}Ca_{1.82}Mg_{4.61}Al_{1.71}Si_{6.86}O_{22}(OH)_2$	$PG_{57}TR_{34}MC_9$	800	4.00	456	$Na_{0.58}Ca_{1.84}Mg_{4.55}Al_{1.75}Si_{6.84}O_{22}(OH)_2$
PARG 19-11	$Na_{0.76}Ca_{1.86}Mg_{4.38}Al_{2.28}Si_{6.48}O_{22}(OH)_2$	$PG_{76}TR_{17}MC_7$	890	1.15	879	$Na_{1.02}Ca_{1.71}Mg_{4.41}Al_{2.24}Si_{6.50}O_{22}(OH)_2$
PARG 11-7	$Na_{0.975}Ca_{1.95}Mg_{4.075}Al_{2.925}Si_{6.05}O_{22}(OH)_2$	$PG_{97.5}TR_0MC_{2.5}$	895	1.32	188	$Na_{0.94}Ca_{1.96}Mg_{4.32}Al_{2.82}Si_{6.00}O_{22}(OH)_2$

Note: Uncertainties in last digit given in parentheses. Data from Sharma and Jenkins (1999).

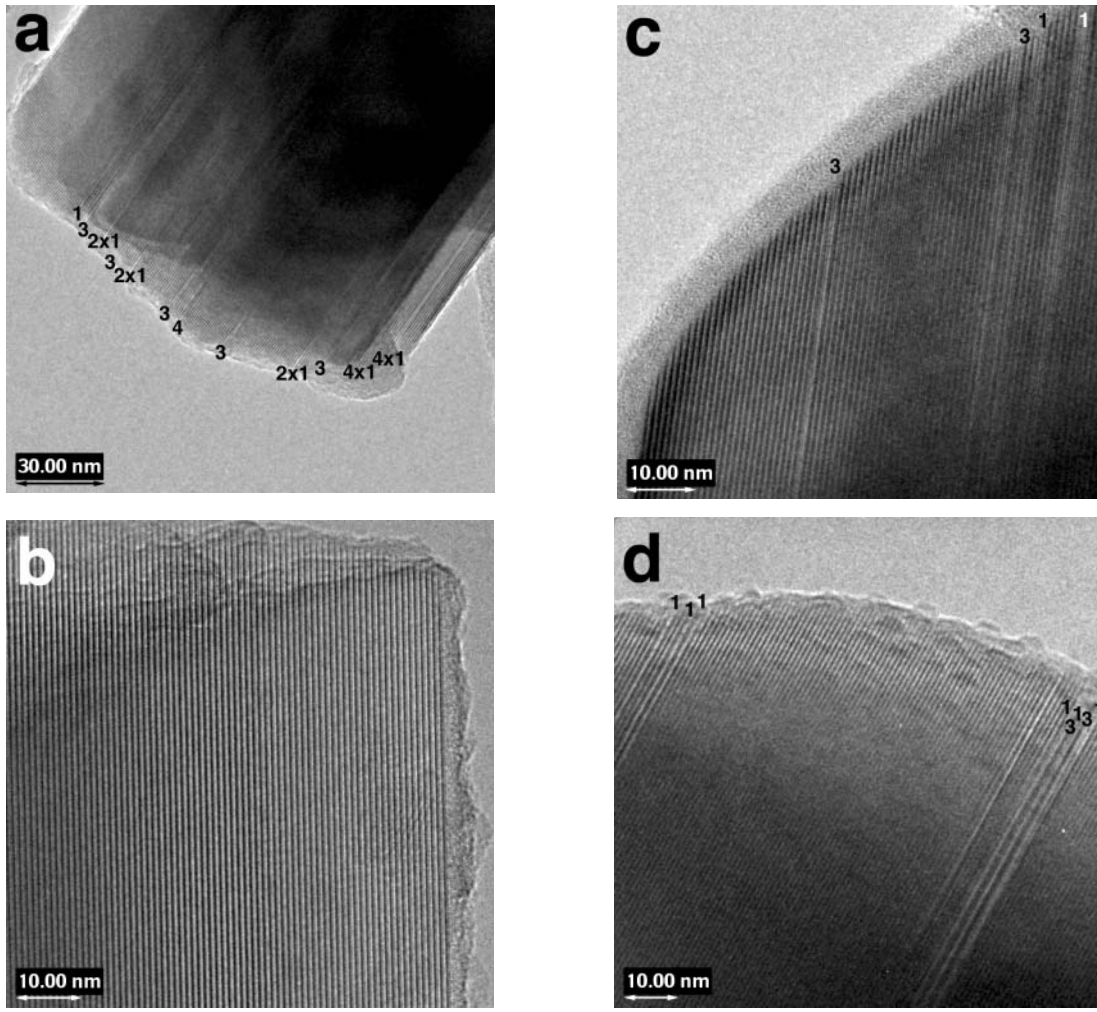

FIGURE 1. Representative HRTEM images taken with the electron beam perpendicular to **b*** of selected amphibole samples synthesized in this study. The multiplicity of defect chains is marked on the images. The number of defect chains in each particular defect slab is shown as a factor in front of the multiplicity, e.g., for a slab of two single chains the symbol is 2×1. (**a**) TREM 23-13 showing isolated single, triple, and quadruple-chain defects. (**b**) PARG 21-2 showing no defects in this crystal. (**c**) PARG 21-2 with several triple and single-chain defects. (**d**) PARG 11-7 showing triple and single-chain defects.

PG), and PARG 11-7 (98 mol% PG). These images show the typical range of defects and their approximate concentrations encountered in these synthetic amphiboles. Although the crystal sizes of these amphiboles are very similar, it was noted that the aspect ratios changed systematically with composition: tremolitic crystals had length-to-width aspect ratios of about 10 while the pargasitic amphiboles had aspect ratios of 5 or less.

Approximately 15 amphibole crystals from each sample shown in Figure 1 were examined in detail for the types and concentrations of CMFs in their structure. CMFs with multiplicities of 1, 3, 4, 5, and 6 were observed. Usually the CMFs occur as individual, isolated slabs one repetition wide along the **b** axis. The dominant CMF is the triple chain, which is noticeably more abundant in the tremolitic sample (TREM 23-13) compared to the other samples. The other (non-triple) CMFs are present at essentially the same concentration in all of the samples and their total concentration is minor (<2%). Statistics for double- and triple-chain concentrations are listed in Table 2. The average double-chain concentrations are tightly clustered at $A'(2)$ values of 0.94–0.96, and the triple-chain concentrations are similarly clustered with $A'(3)$ values of 0.05–0.03. The tremolitic amphibole has the highest defect density.

TABLE 2. Double and triple chain fractions for selected amphiboles from this study

Sample code (mol% PG)	Chain multiplicity fraction and statistics $A'(2)$ ave (1 σ)	max	min	$A'(3)$ ave (1 σ)	n
TREM 23-13 (0% PG)	0.94 (0.05)	0.988	0.889	0.05 (0.04)	15
PARG 21-2 (38% PG)	0.95 (0.05)	1.000	0.849	0.03 (0.03)	14
PARG 11-7 (98% PG)	0.96 (0.02)	0.983	0.941	0.03 (0.01)	17

Note: $A'(i)$ is the ratio of chains of multiplicity i to the sum of all tetrahedral chains in the structure, with an ideal double-chain amphibole having $A'(2) = 1.00$; n = number of crystals measured.

We can now use the concepts of pyribole polysomatism as applied to defect structure description by Veblen and Buseck

(1979), Veblen (1991), and Droop (1994) to calculate directly the amount of Ca and Mg solid solution that occurs in the most defect-rich amphibole TREM 23-13. In brief, amphiboles can be considered as being built of two structural blocks or slabs: a pyroxene (P) slab and a mica (M) slab. In the system CaO-MgO-SiO_2-H_2O, the P slab can be represented by the (doubled) end-member compositions diopside (D = $Ca_2Mg_2Si_4O_{12}$) and enstatite (E = $Mg_2Mg_2Si_4O_{12}$). The M slab has the fixed composition of talc [T = $Mg_3Si_4O_{10}(OH)_2$]. Tremolite, for example, would have one P and one M slab: $Ca_2Mg_2Si_4O_{12} + Mg_3Si_4O_{10}(OH)_2 = Ca_2Mg_5Si_8O_{22}(OH)_2$ (= DT). Compositional variations along the join tremolite-cummingtonite can be expressed as variable substitutions of the D slab for the E slab with no effect on the T slab component of the structure; Ca does not substitute at either the M1-M3 sites of amphibole, the M1 and M2 sites of talc, or the M1 site of pyroxene. Similarly, triple-chain silicates can be represented as a combination of one P slab and two M slabs such as $Ca_2Mg_2Si_4O_{12} + 2Mg_3Si_4O_{10}(OH)_2 = Ca_2Mg_8Si_{12}O_{32}(OH)_4$ (= DTT), which is the postulated calcic analog of clinojimthompsonite (Konishi et al. 1993), or $Mg_2Mg_2Si_4O_{12} + 2Mg_3Si_4O_{10}(OH)_2 = Mg_2Mg_8Si_{12}O_{32}(OH)_4$ (= ETT), which is (clino-) jimthompsonite. Incorporation of wider chain silicates such as MMP (triple chain), MMMP (quadruple chain), or MMMMP (quintuple chain) will change the proportion of the available outer M-sites relative to the inner octahedral sites in the M-slab but will not create any new sites for Ca in the M-slab. If we assume that all of the CMF defects observed in these amphiboles are isolated slabs of unit width, then the outer M-sites will be shared between the amphibole double-chain and the defect slab (M5 sites in clinojimthompsonite). Thus by knowing the bulk composition of a crystal and the amount of the T component, which can be obtained from the HRTEM analysis, we can determine uniquely the amount of Ca-Mg substitution occurring at the outer M-sites.

To illustrate this concept we show a sample calculation for TREM 23-13. From Table 2 we see that TREM 23-13 has 5% triple-chain defects. It is assumed that all of the defects are triple-chains and that the minor abundance of wider-chains (4, 5, and 6) are roughly balanced by single-chain defects (e.g., Ahn et al. 1991). Recasting the triple-chain components on the basis of 23 O atoms, as is done for electron microprobe analyses, one obtains the composition $[Ca,Mg]_{1.97}Mg_{5.02}Si_{8.01}O_{23}(H_2O)_{1.02}$, where the outer M-cations are given in brackets. One can solve for the Ca and Mg content of the outer M-cation sites needed to yield the Ca/Mg ratio of the bulk sample (= 1.82/5.17) to obtain $[Ca_{1.82}Mg_{0.15}]Mg_{5.02}Si_{8.01}O_{23}(H_2O)_{1.02}$. If the triple chain slabs preferentially incorporate Mg into their M5 sites (i.e., are clinojimthompsonite), this would introduce only 0.07 Mg at the outer M-cation sites and an additional 0.08 Mg is needed (equivalent to 4 mol% MC component). If the triple-chain slabs preferentially incorporate Ca at the M5 sites (i.e., Ca-clinojimthompsonite), this would introduce no Mg at the outer M-sites and 0.15 Mg is needed (equivalent to 7.5 mol% MC component). These results indicate that the role of triple-chain defects will be to reduce the apparent 8.5 mol% MC to a true MC content of 4–7.5 mol% for tremolitic amphiboles, and that, regardless of the actual composition of the defects, they alone cannot fully account for the Mg enrichment observed in the tremolite-rich samples.

Similar calculations can be made for pargasitic amphiboles where the mica slab of the structure can be represented by the preiswerkite-like (Pw) composition $NaMg_2Al_3Si_2O_{10}(OH)_2$ and the pyroxene slab is either diopside (D) or enstatite (E) in composition. A Ca-rich triple-chain defect would have the composition DPwPw [= $Na_2Ca_2Mg_6Al_6Si_8O_{32}(OH)_4$]. For pargasite with 3 mol% of the triple-chain defect DPwPw, the composition (based on 23 O atoms) would be $Na_{1.01}Ca_{1.98}Mg_{4.00}Al_{3.03}Si_{5.98}O_{23}(H_2O)_{1.01}$. The calculated composition is in good agreement with the observed Ca content of PARG 11-7 but is in less satisfactory agreement with the observed Mg/Al ratio. The greater chemical complexity of pargasite compared to tremolite and the wider range of possible compositions of the triple chains makes it harder to gauge the influence of triple-chain defects in pargasite-rich amphiboles. However, based on the close match between the predicted and observed Ca contents, we suggest that triple-chain defects may be responsible for the minor deviations from ideal pargasite composition observed by Sharma and Jenkins (1999). This stands in contrast to the tremolite-rich portion of this join.

FTIR spectra

The FTIR absorption spectra in the region of the hydroxyl-stretching vibrations are shown in Figure 2. For tremolite, there is a very sharp band centered at 3674 cm^{-1} with two smaller shoulder bands appearing at slightly lower wavenumbers. Both the sharp band at 3674 cm^{-1} and the lower-frequency shoulder bands have been observed in previous studies (e.g., Hawthorne et al. 1997; Gottschalk et al. 1999; Hawthorne et al. 2000; Melzer et al. 2000, Jenkins et al. 2002) and will be discussed in greater detail below. For pargasite, there are two broad bands of approximately equal intensity centered at 3712 and 3682 cm^{-1}, which is in agreement with earlier studies (e.g., Raudsepp et al. 1987; Welch et al. 1994; Della Ventura et al. 1999; Fialips-Guédon et al. 2000). For the intermediate solid-solutions, the frequencies of the major bands are sufficiently different that they show discrete or separable changes (Farmer 1975) with change in composition. It is of interest to note that the highest frequency band (band A) displays a continuous decrease of ~9 cm^{-1} with increasing PG content.

Figure 3 shows the results of the spectrum-fitting procedure, where a total of 10 bands (A through J) were used to model the absorption spectra for all of the samples. The resultant band positions (in cm^{-1}), band widths (FWHM, in cm^{-1}), and the relative integrated intensities (fraction of the total area) are listed in Table 3. It is emphasized that the set of component bands identified in Figure 3 is not unique but, instead, represents an attempt to model the whole series with a minimum number of bands (e.g., Della Ventura et al. 1999). It should also be noted that the spectrum-fitting procedure was done *independently* of any presumed cation ordering schemes or models.

DISCUSSION

Chain-multiplicity faults

Compared to the tremolitic amphibole studied here, Maresch et al. (1994) synthesized tremolitic amphiboles over a range of

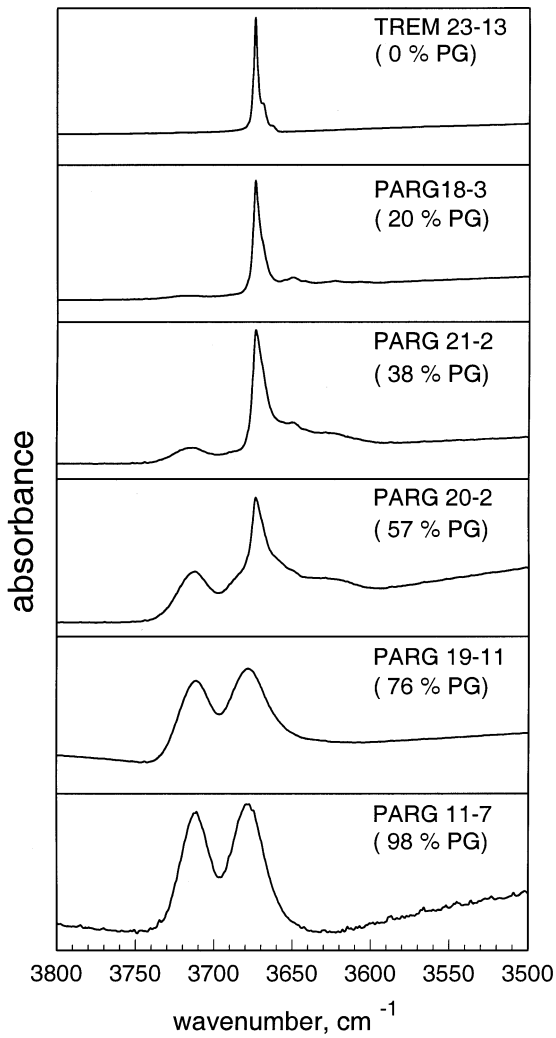

FIGURE 2. FTIR absorption spectra in the region of the hydroxyl-stretching frequencies for the amphibole samples studied here.

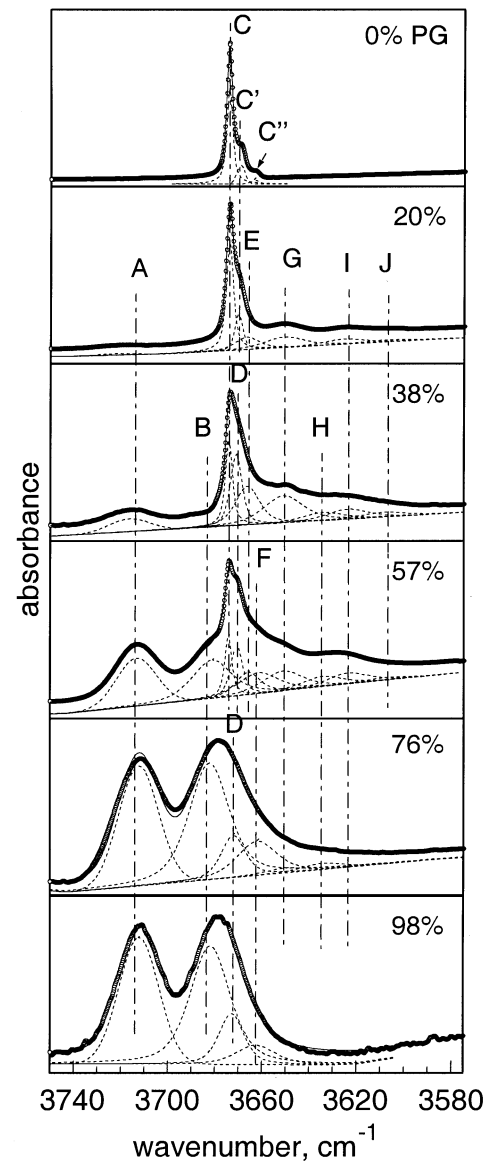

FIGURE 3. Component absorption bands (dashed) identified in this study for the FTIR absorption spectra in Figure 2. The component bands have been shifted slightly to lower intensities to aid their visualization. The total calculated profile is a solid curve and the digitized observed spectra are shown as circles.

pressure-temperature (*P-T*) conditions which they divided into regions I, II, and III. None of the *P-T* conditions used by Maresch et al. (1994) duplicated the conditions used here (800 °C and 4.5 kbar), though their syntheses at 750 °C and 2 kbar or 820 °C and 1 kbar might be considered to be close. The *A*(2) values, which indicate the fraction of undisturbed double-chain volume relative to the entire volume of the pyribole, reported by Maresch et al. (1994) are markedly lower (0.34–0.55) than the *A*'(2) values observed here (0.94–0.96). Although the *A*(2) value tends to be about 0.06–0.08 lower than the *A*'(2) value for the same amphibole, based on the data tabulated by Maresch et al. (1994), this cannot account for the differences in double-chain abundances between the two studies. It has been the experience of the first author that tremolite syntheses at 1–2 kbar vs. 4–6 kbar differ greatly in the kinetics of reactions, in that the higher pressure (denser fluid) appears to enhance the kinetics. This may explain the preservation of precursor phases (talc or diopside) in the study of Maresch et al. (1994) vs. this study. Regardless of the details of the amphibole formation mechanism, it is important to emphasize that defects alone are not responsible for the Mg enrichment of the tremolitic amphibole formed in this study.

With increasing pargasite component, the defect density drops slightly. The sample near the middle of this join (PARG 21-2) showed the largest variability in the defect density from grain to grain. How this variability relates to either its nucleation and growth or bulk composition is not known at this time. Based on this study and that of Ahn et al. (1991), who characterized the CMF contents of synthetic tremolitic amphiboles, there appears to be a direct correlation between aspect ratio and defect density. Smaller aspect ratios imply a more uniform growth rate along all three crystallographic directions, which

TABLE 3. Band position (cm^{-1}), full-width at half maximum values (FWHM, cm^{-1}), and relative intensities (area fraction) of the bands in the hydroxyl-stretching spectra of the synthetic amphiboles studied here

Band	Parameter	Sample					
		TREM 23-13 (0% PG)	PARG 18-3 (20% PG)	PARG 21-2 (38% PG)	PARG 20-2 (57% PG)	PARG 19-11 (76% PG)	PARG 11-7 (98% PG)
A	position	–	3721.7	3716.7	3713.3	3712.5	3712.3
	FWHM	–	20.0	20.0	20.0	20.0	20.0
	intensity	–	0.023	0.085	0.219	0.348	0.387
B	position	–	–	3681.6	3681.5	3682.5	3682.0
	FWHM	–	–	20.0	20.0	20.0	20.0
	intensity	–	–	0.009	0.207	0.404	0.427
C	position	3674.3	3674.2	3674.4	3674.5	–	–
	FWHM	3.0	3.6	3.6	3.6	–	–
	intensity	0.805	0.395	0.140	0.066	–	–
C'	position	3669.5	3670.3	–	–	–	–
	FWHM	4.0	4.0	–	–	–	–
	intensity	0.162	0.132	–	–	–	–
C''	position	3663.6	–	–	–	–	–
	FWHM	4.0	–	–	–	–	–
	intensity	0.033	–	–	–	–	–
D	position	–	–	3671.4	3671.0	3672.3	3672.8
	FWHM	–	–	6.0	6.0	12.1	12.5
	intensity	–	–	0.174	0.084	0.089	0.117
E	position	–	3666.8	3666.6	3666.1	–	–
	FWHM	–	12.0	12.0	12.0	–	–
	intensity	–	0.134	0.189	0.075	–	–
F	position	–	–	–	3661.7	3662.2	3662.6
	FWHM	–	–	–	20.0	20.0	20.0
	intensity	–	–	–	0.111	0.119	0.069
G	position	–	3650.8	3651.3	3651.2	3650.1	–
	FWHM	–	20.0	20.0	20.0	20.0	–
	intensity	–	0.187	0.216	0.109	0.017	–
H	position	–	–	3634.3	3634.3	3634.3	–
	FWHM	–	–	20.0	20.0	20.0	–
	intensity	–	–	0.064	0.055	0.021	–
I	position	–	3625.3	3623.9	3623.7	3623.7	–
	FWHM	–	20.0	20.0	20.0	20.0	–
	intensity	–	0.090	0.079	0.059	0.001	–
J	position	–	3607.5	3608.9	3608.7	–	–
	FWHM	–	23.0	23.0	23.0	–	–
	intensity	–	0.038	0.042	0.014	–	–

appears to produce fewer CMF defects. Because the amphiboles examined in this study were formed over a limited range of temperature (800–900 °C) and pressure (1–4 kbar), it is suggested that incorporation of the pargasite component is the main factor influencing the defect density. Incorporation of other components into tremolite, such as aluminotschermakite (Ahn et al. 1991; Smelik et al. 1994) and richterite (Pawley et al. 1993), appears to reduce the defect density and, if reported, the aspect ratio.

Cation site occupancies

To interpret the FTIR spectra, it is important to review what is known about the cation site occupancies of the amphiboles under investigation here. As reported by Sharma and Jenkins (1999), direct electron-microprobe analysis of representative amphibole crystals from each synthesis confirm that the principal chemical substitutions of ^{VI}Al for ^{VI}Mg, ^{IV}Al for ^{IV}Si, and Na for a vacancy at the A site are closely followed. The one notable exception is sample PARG 19-11 (76% PG component) which has an abnormally high Na content. The cause of this high Na content is not known (Sharma and Jenkins 1999), and would not be expected given that the ratio of ^{VI}Al to ^{IV}Al agrees with the pargasite substitution.

The neutron-diffraction study of synthetic (OH-) pargasite reported by Welch and Knight (1999) provides a valuable reference for predicting the distribution of Al, Mg, and Si in the samples reported here. Although Al generally occurs at the M2 and T1 sites, Welch and Knight (1999) reported more disorder than this, with 50% of the octahedral Al occurring at the M3 site and 14% of the tetrahedral Al occurring at the T2 site. The presence of Al over more than one octahedral site has been shown by single-crystal structure refinements of natural pargasite (Oberti et al. 1995), by the NMR spectra of synthetic pargasite (Welch et al. 1994), and by the NMR spectra of amphiboles synthesized along the tremolite-aluminotschermakite join (Jenkins et al. 1997; Hawthorne et al. 2000). Similarly, the presence of Si-Al disorder over both the T1 and T2 sites is supported, though indirectly, by modeling the intensities of the complex ^{29}Si MAS-NMR spectra of synthetic pargasite (Welch et al. 1998) and of synthetic tremolite-tschermakite solid solutions (Jenkins et al. 1997). It will be assumed that the long-range cation distribution for the amphiboles studied here vary linearly between that of pargasite and tremolite. The estimated T- and M-site occupancies based on this assumption are given in Table 4.

Sodium substitution into the A site can occur over a variety of positions, such as at the intersection of the twofold rotation axis and the mirror plane (A2/*m*), at various positions within the mirror plane (A*m*), or at various positions along the rotation axis (A2). Sharma and Jenkins (1999) simply assumed that Na occurs at the *A*2/*m* position. Welch and Knight (1999) were unable to refine Na occupancies at the split A sites for syn-

TABLE 4. Estimated cation site occupancies in atoms per formula unit for the amphiboles studied here

Sample	^{IV}Si	Al_{total}	$^{IV}Al^{T1*}$	$^{IV}Al^{T2*}$	^{VI}Al	$^{VI}Al^{M2*}$	$^{VI}Al^{M3*}$	Ca^{M4}	Na^{A}
TREM 23-13	8.00	0.0	0.0	0.0	0.0	0.0	0.0	1.82	0.0
PARG 18-3	7.67	0.52	0.28	0.05	0.19	0.095	0.095	1.86	0.14
PARG 21-2	7.19	1.23	0.69	0.11	0.42	0.21	0.21	1.67	0.43
PARG 20-2	6.84	1.75	0.99	0.16	0.59	0.295	0.295	1.84	0.58
PARG 19-11	6.50	2.24	1.29	0.21	0.74	0.37	0.37	1.71	1.02
PARG 11-7	6.00	2.82	1.72	0.28	0.82	0.41	0.41	1.96	0.94

Note: ^{IV}Si, Al_{total}, ^{VI}Al, Ca, and Na contents are from Table 1. Si constitutes the remainder of the T1 and T2 sites while Mg constitutes the remainder of the M2, M3, and M4 sites.

* Occupancies determined by a linear interpolation between tremolite and the site occupancies reported by Welch and Knight (1999) for synthetic pargasite.

thetic pargasite from the neutron powder-diffraction pattern, but they could confirm Na had a large degree of positional disorder at this site. Based on the single-crystal refinements of a suite of A-site containing amphiboles reported by Hawthorne et al. (1996b) and the gem-quality pargasite (with minor F and K) reported by Tait et al. (2001), Na in pargasitic amphiboles free of K and F is expected to be strongly ordered at the A2 site.

Cation configuration assignments to the FTIR bands

Although some theoretical attempts have been made to calculate the dependency of the OH-stretching frequency on composition (e.g., Abbott 1991), empirical observations have generally proven more reliable for interpreting shifts in the OH-stretching frequency. We are now in a position to use the relatively large amount of work that has been done in recent years on chemically simplified amphibole joins to assign specific cation configurations to the bands identified in Figure 3. Of particular relevance are the studies of the joins tremolite-potassium-richterite (Hawthorne et al. 1997), tremolite-cummingtonite (Gottschalk et al. 1999), richterite-pargasite (Della Ventura et al. 1999), and tremolite-aluminotschermakite (Hawthorne et al. 2000). One can refer to the discussions presented in these studies, which correlate observed shifts in the OH-stretching frequency resulting from simple chemical substitutions with short-range cation configurations that are most favorable on the basis of bond-valence theory (e.g., Hawthorne 1997), to better understand the background for the following band assignments. The component bands will be considered in the order in which they appear most intensely with increasing PG component: band C (with C' and C''), followed by bands D-J, which correspond to some of the same bands observed for aluminous tremolite by Hawthorne et al. (2000), and finally bands A and B which correspond to some of the same bands observed along the tremolite-richterite join by Della Ventura et al. (1999). Cation configurations for amphiboles in this study will be indicated in a similar fashion to that used by Della Ventura et al. (1999), namely, M1M1M3-OH-A:T1T1-M2M2M3-M2M2-M4M4, where the M-sites to the right of the T1 sites are next-nearest-neighbor M2 and M3 sites. The next-next-nearest-neighbor M4 sites have been included because the cation occupancies at these sites have a perceptible influence on some of the principal bands.

Band C. As noted above, band C at 3674 cm^{-1} has been observed in previous studies and is generally attributed to the configuration MgMgMg-OH-□:SiSi-MgMgMg-MgMg-CaCa in tremolite. The two clearly identifiable shoulder bands at 3669 and 3664 cm^{-1} marked C' and C'' respectively, have been attributed to the substitution of Mg for Ca at the M4 sites, i.e., attributed to the presence of the true MC component in TREM 23-13 documented in this study. This agrees with the observation made by Burns and Strens (1966) where the MgMgMg band in (high-Ca) tremolite shifts from 3673 cm^{-1} to 3665 cm^{-1} in (low-Ca) cummingtonite. A brief examination of the relative band intensities predicted for random mixing helps support the assignment of these shoulder bands to substitutions of Mg for Ca at the M4 sites. For tremolitic amphibole with a maximum of 7.5 mol% MC component ($^{M4}X_{Mg} = 0.075$), one would calculate the proportion of sites occupied only by Ca (= C = $^{M4}X_{Ca}{}^{2}$), by Ca + Mg (= C' = $2 \cdot {}^{M4}X_{Ca} \cdot {}^{M4}X_{Mg}$), and only by Mg (= C'' = $^{M4}X_{Mg}{}^{2}$) to be 0.856, 0.139, and 0.006, respectively. The relative band intensities observed in this study are 0.805, 0.162, and 0.033, respectively, suggesting that there is either a higher proportion of the MC component in TREM 23-13 than observed (closer to 10 mol% MC) or that the C, C', and C'' absorption bands actually involve the two closest (H-M4 at a distance of ~5.5 Å) *and* the two more distant (H-M4' at ~5.7 Å) sites in the next unit cell along the octahedral slab (Hawthorne and Grundy 1976). The former suggestion of having more than 7.5 mol% MC component is not supported by the TEM analyses presented here. The latter suggestion, however, is quite feasible because of the small difference between the distances of the two sets of M4 sites from the hydrogen atom. Gottschalk et al. (1999) explicitly considered this case and presented the equations for calculating the probabilities of the various CaCaCaCa, CaCaCaMg, and CaCaMgMg configurations. For tremolite with 5 mol% MC component (within the range observed in this study), the probabilities of these configurations are 0.814, 0.171, and 0.014, respectively, if one combines the probabilities of the "nearer" and "further" M4 sites (Gottschalk et al. 1999). The close agreement between these calculated band intensities and the intensities observed here for tremolitic amphibole supports the hypothesis that the shoulders on the dominant C band are influenced by the closest four, and not just the closest two, M4 sites. The cation configurations for bands C, C', and C'' in Table 5 indicate the cation combinations at both the nearer and further M4 sites.

The minor shoulder bands C' and C'' are not easily resolved with increasing pargasite content because of increasing band overlap and band broadening. Only band C' was identified in PARG 18-3, primarily because of this band's high intensity in TREM 23-13 and the low PG content in PARG 18-3. Although bands D and E listed in Table 3 are at about the same positions as C' and C'', respectively, the significant shift in band position and increase in width for C' beginning at 38% PG (PARG 21-

TABLE 5. Observed vibration bands and their assigned cation configurations

No.	Band	Assigned configuration* *M1M1M3-OH-A:T1T1-M2M2M3-M2M2-M4M4*	Position (cm^{-1})	Source†
1	A	MgMgMg-OH-Na:SiAl-MgMgMg-MgMg-CaCa	3721–3712	B of D (1999)
2	B	MgMgAl-OH-Na:SiAl-MgMgMg-MgMg-CaCa	3681	D of D (1999)
3	C	MgMgMg-OH-□:SiSi-MgMgMg-MgMg-CaCaCaCa	3674	A of H (2000)
4	C'	MgMgMg-OH-□:SiSi-MgMgMg-MgMg-CaMgCaCa	3669	B of G (1999)
5	C''	MgMgMg-OH-□:SiSi-MgMgMg-MgMg-MgMgCaCa	3664	D of G (1999)
6	D	MgMgMg-OH-□:SiSi-AlMgMg-MgMg-CaCa	3671	A' of H (2000)
7	D	MgMgMg-OH-□:SiSi-MgMgAl-MgMg-CaCa	3671	A' of H (2000)
8	D	MgMgAl-OH-Na:SiAl-AlMgMg-MgMg-CaCa	3671	F of D (1999)
9	E	MgMgMg-OH-□:SiSi-MgMgMg-MgMg-MgMg	3666	A' of BS (1966)
10	F	MgMgAl-OH-Na:SiAl-AlMgMg-AlMg-CaCa	3662	G of D (1999)
11	F	MgMgMg-OH-□:SiSi-AlMgMg-MgMg-MgMg	3662	this study
12	F	MgMgMg-OH-□:SiSi-MgMgAl-MgMg-MgMg	3662	this study
13	G	MgMgMg-OH-□:SiAl-MgMgMg-MgMg-CaCa	3650	B of H (2000)
14	H	MgMgAl-OH-□:SiSi-MgMgMg-MgMg-CaCa	3634	B' of H (2000)
15	H	MgMgMg-OH-□:SiAl-AlMgMg-MgMg-CaCa	3634	B' of H (2000)
16	H	MgMgMg-OH-□:SiAl-MgMgAl-MgMg-CaCa	3634	B' of H (2000)
17	I	MgMgAl-OH-□:SiSi-AlMgMg-MgMg-CaCa	3625	C of H (2000)
18	I	MgMgAl-OH-□:SiSi-MgMgAl-MgMg-CaCa	3625	C of H (2000)
19	I	MgMgAl-OH-□:SiAl-MgMgMg-MgMg-CaCa	3625	C of H (2000)
20	J	MgMgAl-OH-□:SiAl-AlMgMg-MgMg-CaCa	3609	C' of H (2000)
21	J	*MgMgAl-OH-□:SiAl-MgMgAl-MgMg-CaCa*	3609	C' of H (2000)

* The configuration notation indicates the cations at the three nearest-neighbor octahedra (M1M1M3) to the OH site, the A-site occupancy (Na or a void, □), the cations at the T1 dimers associated with the OH site, the five next-nearest neighbor sites (M2M2M3-M2M2), and the two nearest M4 sites. For the C, C', and C'' bands the last four cations indicate the combinations considered at both the two nearest and two furthest M4 sites (see text).

† Source abbreviations: BS (1966) = Burns and Strens (1966); D (1999) = Della Ventura et al. (1999); G (1999) = Gottschalk et al. (1999); H (2000) = Hawthorne et al. (2000).

2) and the increase in band width for C'' beginning at 20% PG (PARG 18-3) makes it difficult to justify that these are due to the same absorption.

Bands D-J. Bands D-J appear at lower frequencies than band C and are considered to be influenced by three main compositional substitutions: Al for Mg and Si at sites adjacent to vacant A-sites; Al for Mg and Si at sites adjacent to occupied A-sites; and Mg for Ca at the two nearest M4 sites.

At low PG contents, the low-frequency portion of the spectrum bears a close resemblance to the spectra of aluminous tremolites reported by Hawthorne et al. (2000). Bands G, H, I, and J in particular correspond closely in position and intensity to bands B, B', C, and C' of Hawthorne et al. (2000). These bands are therefore attributed to cation configurations associated with a vacant A-site and which involve the substitution of Al for Mg and Si, as listed in Table 5. Notice that bands H, I, and J have several configurations listed because these structurally distinct short-range configurations are considered spectroscopically indistinguishable (Hawthorne et al. 2000).

Bands D and F appear about midway along the compositional join and persist all the way through the pargasite endmember. These bands are attributed in part to cation configurations associated with Na at the A site; however, to achieve such low vibration frequencies, these configurations must involve substantial Al substitution for Mg and Si. A variety of such configurations were proposed by Della Ventura et al. (1999). Band D at 3671 cm^{-1} of this study corresponds closely in position and intensity to band F of Della Ventura et al. (1999). Band D of this study also corresponds closely to band A' of Hawthorne et al. (2000), which is attributed to the substitution of Al for Mg at either the next-nearest M2 or M3 site (either being indistinguishable from the other) in the A-site vacant configuration MgMgMg-OH-□:SiSi-MgMgMg-MgMg-CaCa. This suggests that A-site vacant configurations will contribute to this band at lower PG contents. Band F of this study correlates most closely in its relative, rather than absolute, position to band G of Della Ventura et al. (1999). This assignment is complicated by the fact that, in both this study and that of Della Ventura et al. (1999), this band occurs as a minor component of the low-frequency tail of the broad absorption envelope centered at about 3680 cm^{-1} in pargasite. As a result, the location of this band is not so well defined and is strongly influenced by the overall choice of bands used to fit the spectrum of pargasite (four bands in this study compared to six bands used by Della Ventura et al. 1999). It is also proposed below that a portion of band F is influenced by Mg substitution at the M4 sites.

Finally, two bands in the low-frequency portion of the spectra are attributed to the presence of Mg at the M4 sites. Band E at 3666 cm^{-1} occurs at essentially the same frequency as the (low-Ca) cummingtonite MgMgMg band observed by Burns and Strens (1966) and is, therefore, assigned to the configuration MgMgMg-OH-□:SiSi-MgMgMg-MgMg-MgMg. Assignment of band E to this configuration is supported by (1) its near coincidence with the vibration frequency of band C'' in the 0% PG sample (Fig. 3), which is assigned to the same configuration, and (2) by its presence in samples with the highest MC contents (Table 1). Indeed, it is only because of the differences in the half-widths of E and C'', which are 12 and 4 cm^{-1}, respectively, that they are considered different bands. The greater width of band E probably arises from the greater short-range compositional disorder present in the amphiboles near the middle of the join. In the same fashion that substitution of Mg at the M4 site shifts band C by –8 cm^{-1} to 3666 cm^{-1}, so also it is possible that this substitution can shift band D by –8 cm^{-1} to 3662 cm^{-1}, which is the position of band F. It is proposed here that band F is the sum of at least two types of configurations, those involving A-site-occupied configurations (no. 10 in Table 5) and those involving A-site-vacant configura-

tions (nos. 11 and 12 in Table 5), the latter stemming from the substitution of Mg at the M4 site of the A-site-vacant configurations identified for band D (nos. 6 and 7 in Table 5). The contribution of A-site-vacant configurations 11 and 12 to band F helps explain why the intensity of this band decreases with increasing PG content.

Bands A and B. Traditionally band A at about 3712 cm^{-1} in pargasite has been attributed to the configuration MgMgMg-OH-Na:SiSi-MgMgMg-MgMg-CaCa (e.g., Raudsepp et al. 1987; Welch et al. 1994; Fialips-Guédon et al. 2000). However, Della Ventura et al. (1999) showed that this configuration is associated with the higher-frequency absorption band observed for (Al-free) richterite at about 3730 cm^{-1}, and that the band at 3712 cm^{-1} is instead attributed to the presence of Al at one of the T1 sites in the configuration MgMgMg-OH-Na:SiAl-MgMgMg-MgMg-CaCa. The association of Na with tetrahedral Al is supported by the bond-valence analysis of pargasite by Hawthorne (1997), which predicts that Na at the A2 site is locally associated with Al at the T1 site. We have adopted this assignment for band A in this study and indicate this as configuration 1 in Table 5. Only one broad peak was fitted to the A band (3712 cm^{-1}) for pargasite because the fitting procedure was done independently of any cation-configuration model; however, it is possible to fit this broad absorption maximum with two component bands (3716 and 3705 cm^{-1}), as was done by Della Ventura et al. (1999), with the lower-frequency band being attributed to the configuration MgMgMg-OH-Na:SiAl-AlMgMg-MgMg-CaCa (Al at the M2 site).

It has been shown that substitution of other trivalent cations for $^{[VI]}$Al in pargasite produces a noticeable shift in band B but not in band A (e.g., Raudsepp et al. 1987; Fialips-Guédon et al. 2000). Furthermore, the peculiar splitting that occurs in band B when Cr is gradually added to pargasite (Fialips-Guédon et al. 2000) has been attributed to the substitution of Cr for Al at the nearest-neighbor M3 site. Accordingly, we adopt the assignment of band B in this study to the configuration proposed for band D in the study of Della Ventura et al. (1999), which involves Al at the nearest-neighbor M3 site.

Short-range order

Because infrared spectroscopy is sensitive to short-range configurations, it should be possible to use the OH-stretching band interpretations presented above along with probability theory to test for the presence of short-range cation order. The approach taken here is to compare the theoretical intensities (random-mixing probabilities) of a given configuration to the observed intensities to see how closely they agree, similar to what was done above for band C. The accuracy of this analysis depends on (1) independent knowledge of the long-range ordering of cations, (2) correct assignment of cation configurations to specific absorption bands, and (3) allowance for any variations in molar absorptivity of the bands across the wavenumber range of interest (Hawthorne et al. 1996a). The first two issues have been discussed above while the third has been discussed at length in previous articles (Skogby and Rossman 1991; Della Ventura et al. 1996; Hawthorne et al. 1997). It was shown by Skogby and Rossman (1991) that the molar absorptivity of the OH-stretching bands increases linearly with decreasing frequency when measured on oriented single-crystals of amphibole. Subsequent testing of this relationship using the FTIR spectra measured with amphibole powders has either shown that molar absorptivity is constant (Della Ventura et al. 1996) or varies less strongly (Hawthorne et al. 1997) than reported by Skogby and Rossman (1991). While the exact magnitude of this effect is still a matter of speculation, we have adopted the original molar-absorptivity-to-wavenumber correlation proposed by Skogby and Rossman (1991) and use the technique proposed by Della Ventura et al. (1996) of normalizing all of the observed band intensities (I_i^{obs}) to the wavelength of the highest-frequency band (band A) within a given spectrum. The corrected band intensities (I_i^{cor}) are calculated from the equation:

$$I_i^{cor} = I_i^{obs}(\varepsilon_A / \varepsilon_i)$$

where $\varepsilon_A/\varepsilon_i$ is the ratio of the molar absorptivities of band A and the band of interest (i) from Figure 4 of Skogby and Rossman (1991).

Table 6 gives the equations for random mixing probabilities which were used to calculate the theoretical band intensities for each of the cation configurations that were identified in this study (Table 5). To look for general trends in cation clus-

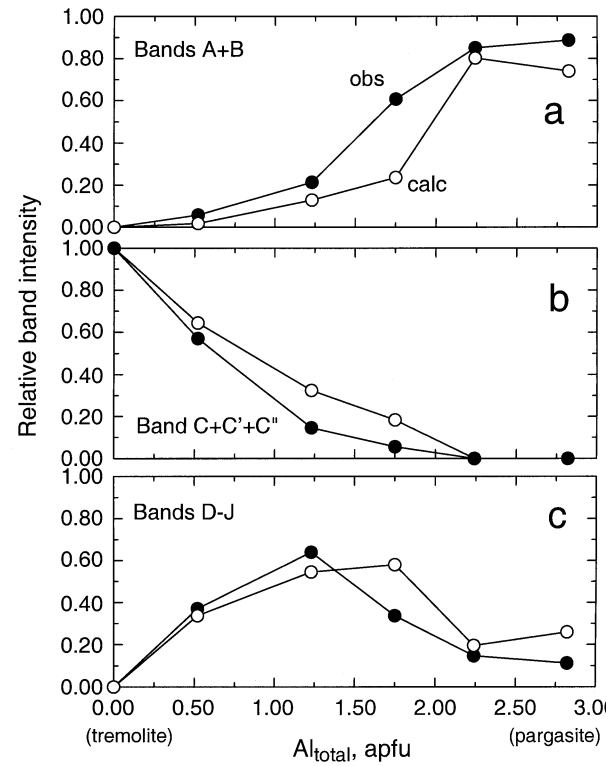

FIGURE 4. Comparison of the observed intensities (solid symbols) and the calculated intensities (open symbols) of the OH-stretching bands identified in this study, with both sets of intensities being normalized to a total area of 1.0, shown as a function of the total Al content in the samples in atoms per formula unit (apfu). (**a**) Bands A + B. (**b**) Band C (+ C' + C" where present, Table 3). (**c**) Sum of bands D through J.

tering, bands A and B were considered together because of their dependence on A-site Na, band C (along with C' and C'') closely represents bands attributed to the tremolite component, and bands D through J largely depend on A-site vacant configurations involving the substitution of Al at tetrahedral and octahedral sites. Figure 4 shows the calculated intensities (open symbols) for bands A + B, C + C' + C'', and D-J, normalized to a total area of 1.0, as a function of total Al atoms per formula unit (apfu) in the amphibole. Also shown in Figure 4 are the observed intensities (solid symbols) corrected for differences in molar absorptivity. The observed intensities of bands A + B in Figure 4a are consistently higher than their calculated intensities, with a factor of three discrepancy occurring at an Al_{total} content of 1.75 (PARG 20-2, 57% PG). The observed "tremolite" configuration bands (C + C' + C'', Fig. 4b) are lower by a factor of two than the expected intensities near the middle of the join. Bands D-J in Figure 4c generally follow the same trend but show a peculiar reversal near the middle of the join, with the observed intensities changing from being higher to lower than expected with increasing Al content. The greatest discrepancy (factor of two) for bands D-J is again at an Al_{total} content of 1.75.

Though not definitive, these observations suggest the manner in which the actual thermodynamic activities of specific amphibole components may deviate from the calculated ideal activities. Qualitatively, ideal activities calculated from random-mixing of cations over a certain number of sites will increase as the degree of random mixing (entropy of mixing) decreases either in response to local-charge balance considerations (e.g., Wood and Fraser 1976, p. 95ff) or, more quantitatively, in response to short-range order imposed by bond-valence constraints (Hawthorne 1997). One can see from Figure 4a that the intensities of cation configurations involving A-site Na, $^{[IV]}$Al, and $^{[VI]}$Al (bands A + B) are stronger than those predicted from random-mixing statistics, implying some degree of short-range ordering for these configurations. Accordingly, the activities of amphibole components based on these configurations, such as the pargasite component, should be greater than what one would predict from random-mixing models. Similarly, from Figure 4b, one would predict the activity of the tremolite component to be lower than expected from random-mixing models. The peculiar cross-over in the observed and calculated curves of Figure 4c suggests that the activities of components involving a vacant A-site, $^{[IV]}$Al, and $^{[VI]}$Al (bands D-J), such as aluminotschermakite or

TABLE 6. Probabilities of cation configurations associated with the bands identified in Table 5

No.	Band	Probability
1	A	$(X_{Mg}^{M1})^2(X_{Mg}^{M3})(X_{Na}^{A})(X_{Si}^{T1})(X_{Al}^{T1})\cdot 2\cdot(X_{Mg}^{M2})^2(X_{Mg}^{M3})(X_{Mg}^{M2})^2(X_{Ca}^{M4})^2$
2	B	$(X_{Mg}^{M1})^2(X_{Al}^{M3})(X_{Na}^{A})(X_{Si}^{T1})(X_{Al}^{T1})\cdot 2\cdot(X_{Mg}^{M2})^2(X_{Mg}^{M3})(X_{Mg}^{M2})^2(X_{Ca}^{M4})^2$
3	C	$(X_{Mg}^{M1})^2(X_{Mg}^{M3})(X_{\square}^{A})(X_{Si}^{T1})^2(X_{Mg}^{M2})^2(X_{Mg}^{M3})(X_{Mg}^{M2})^2(X_{Ca}^{M4})^2$
4	C'	$(X_{Mg}^{M1})^2(X_{Mg}^{M3})(X_{\square}^{A})(X_{Si}^{T1})^2(X_{Mg}^{M2})^2(X_{Mg}^{M3})(X_{Mg}^{M2})^2(X_{Ca}^{M4})(X_{Mg}^{M4})\cdot 2$
5	C''	$(X_{Mg}^{M1})^2(X_{Mg}^{M3})(X_{\square}^{A})(X_{Si}^{T1})^2(X_{Mg}^{M2})^2(X_{Mg}^{M3})(X_{Mg}^{M2})^2(X_{Mg}^{M4})^2$
6	D	$(X_{Mg}^{M1})^2(X_{Mg}^{M3})(X_{\square}^{A})(X_{Si}^{T1})^2(X_{Al}^{M2})(X_{Mg}^{M2})\cdot 2\cdot(X_{Mg}^{M3})(X_{Mg}^{M2})^2(X_{Ca}^{M4})^2$
7	D	$(X_{Mg}^{M1})^2(X_{Mg}^{M3})(X_{\square}^{A})(X_{Si}^{T1})^2(X_{Mg}^{M2})^2(X_{Al}^{M3})(X_{Mg}^{M2})^2(X_{Ca}^{M4})^2$
8	D	$(X_{Mg}^{M1})^2(X_{Al}^{M3})(X_{Na}^{A})(X_{Si}^{T1})(X_{Al}^{T1})\cdot 2\cdot(X_{Al}^{M2})(X_{Mg}^{M2})\cdot 2\cdot(X_{Mg}^{M3})(X_{Mg}^{M2})^2(X_{Ca}^{M4})^2$
9	E	$(X_{Mg}^{M1})^2(X_{Mg}^{M3})(X_{\square}^{A})(X_{Si}^{T1})^2(X_{Mg}^{M2})^2(X_{Mg}^{M3})(X_{Mg}^{M2})^2(X_{Mg}^{M4})^2$
10	F	$(X_{Mg}^{M1})^2(X_{Al}^{M3})(X_{Na}^{A})(X_{Si}^{T1})(X_{Al}^{T1})\cdot 2\cdot(X_{Al}^{M2})(X_{Mg}^{M2})\cdot 2\cdot(X_{Mg}^{M3})(X_{Al}^{M2})(X_{Mg}^{M2})\cdot 2\cdot(X_{Ca}^{M4})^2$
11	F	$(X_{Mg}^{M1})^2(X_{Mg}^{M3})(X_{\square}^{A})(X_{Si}^{T1})^2(X_{Al}^{M2})(X_{Mg}^{M2})\cdot 2\cdot(X_{Mg}^{M3})(X_{Mg}^{M2})^2(X_{Mg}^{M4})^2$
12	F	$(X_{Mg}^{M1})^2(X_{Mg}^{M3})(X_{\square}^{A})(X_{Si}^{T1})^2(X_{Mg}^{M2})^2(X_{Al}^{M3})(X_{Mg}^{M2})^2(X_{Mg}^{M4})^2$
13	G	$(X_{Mg}^{M1})^2(X_{Mg}^{M3})(X_{\square}^{A})(X_{Si}^{T1})(X_{Al}^{T1})\cdot 2\cdot(X_{Mg}^{M2})^2(X_{Mg}^{M3})(X_{Mg}^{M2})^2(X_{Ca}^{M4})^2$
14	H	$(X_{Mg}^{M1})^2(X_{Al}^{M3})(X_{\square}^{A})(X_{Si}^{T1})^2(X_{Mg}^{M2})^2(X_{Mg}^{M3})(X_{Mg}^{M2})^2(X_{Ca}^{M4})^2$
15	H	$(X_{Mg}^{M1})^2(X_{Mg}^{M3})(X_{\square}^{A})(X_{Si}^{T1})(X_{Al}^{T1})\cdot 2\cdot(X_{Al}^{M2})(X_{Mg}^{M2})\cdot 2\cdot(X_{Mg}^{M3})(X_{Mg}^{M2})^2(X_{Ca}^{M4})^2$
16	H	$(X_{Mg}^{M1})^2(X_{Mg}^{M3})(X_{\square}^{A})(X_{Si}^{T1})(X_{Al}^{T1})\cdot 2\cdot(X_{Mg}^{M2})^2(X_{Al}^{M3})(X_{Mg}^{M2})^2(X_{Ca}^{M4})^2$
17	I	$(X_{Mg}^{M1})^2(X_{Al}^{M3})(X_{\square}^{A})(X_{Si}^{T1})^2(X_{Al}^{M2})(X_{Mg}^{M2})\cdot 2\cdot(X_{Mg}^{M3})(X_{Mg}^{M2})^2(X_{Ca}^{M4})^2$
18	I	$(X_{Mg}^{M1})^2(X_{Al}^{M3})(X_{\square}^{A})(X_{Si}^{T1})^2(X_{Mg}^{M2})^2(X_{Al}^{M3})(X_{Mg}^{M2})^2(X_{Ca}^{M4})^2$
19	I	$(X_{Mg}^{M1})^2(X_{Al}^{M3})(X_{\square}^{A})(X_{Si}^{T1})(X_{Al}^{Si})\cdot 2\cdot(X_{Mg}^{M2})^2(X_{Al}^{M3})(X_{Mg}^{M2})^2(X_{Ca}^{M4})^2$
20	J	$(X_{Mg}^{M1})^2(X_{Al}^{M3})(X_{\square}^{A})(X_{Si}^{T1})(X_{Al}^{Si})\cdot 2\cdot(X_{Al}^{M2})(X_{Mg}^{M2})\cdot 2\cdot(X_{Mg}^{M3})(X_{Mg}^{M2})^2(X_{Ca}^{M4})^2$
21	J	$(X_{Mg}^{M1})^2(X_{Al}^{M3})(X_{\square}^{A})(X_{Si}^{T1})(X_{Al}^{Si})\cdot 2\cdot(X_{Mg}^{M2})^2(X_{Al}^{M3})(X_{Mg}^{M2})^2(X_{Ca}^{M4})^2$

Note: X_j^k = the mole fraction of cation j at site k.

magnesiohornblende, may show a reversal from having higher than expected to lower than expected activities approximately mid-way along the tremolite-pargasite join. As our ability to interpret the fine structure of the OH-stretching vibrations of amphibole continues to improve, we may be able to use this analytical tool to better understand the effects that short-range order have on the macroscopic properties of amphibole solid solutions.

ACKNOWLEDGMENTS

We appreciate the thorough review of the original manuscript by F.C. Hawthorne. We gratefully acknowledge financial support from NSF grant EAR-9909452 to D.M.J.

REFERENCES CITED

Abbott, R.N. Jr. (1991) A short-range O-H potential for amphiboles based on OH-stretching frequencies. Canadian Mineralogist, 29, 131–142.

Ahn, J.H., Cho, M., Jenkins, D.M., and Buseck, P.R. (1991) Structural defects in synthetic tremolitic amphiboles. American Mineralogist, 76, 1811–1823.

Bozhilov, K.N. (1997) Transmission electron microscopy study of crystal growth, solid solution and defect formation: hollandite and synthetic tremolite. Ph.D. Dissertation, Johns Hopkins University, 157 pp.

Bozhilov, K.N., Green, H.W., and Dobrzhinetskaya, L. (1999) Clinoenstatite in Alpe Arami peridotite: Additional evidence of very high pressure. Science, 284, 128–132.

Burns, R.G. and Strens, R.G.J. (1966) Infrared study of the hydroxyl bands in clinoamphiboles. Science, 153, 890–892.

Della Ventura, G., Robert, J.-L., and Hawthorne, F. C. (1996) Infrared spectroscopy of synthetic (Ni, Mg, Co)-potassium-richterite. In M. D. Dyar, C. McCammon, and M. W. Schaefer, Eds., Mineral spectroscopy, a tribute to Roger G. Burns, Geochemical Society Special Publication 5, p. 55–63.

Della Ventura, G., Hawthorne, F.C., Robert, J.-L., Delbove, F., Welch, M.F., and Raudsepp, M. (1999) Short-range order of cations in synthetic amphiboles along the richterite-pargasite join. European Journal of Mineralogy, 11, 79–94.

Della Ventura, G., Robert, J.-L., Sergent, J., Hawthorne, F.C., and Delbove, F. (2001) Constraints on F vs. OH incorporation in synthetic $^{[6]}$Al-bearing monoclinic amphiboles. European Journal of Mineralogy, 13, 841–847.

Droop, G.T.R. (1994) Triple-chain pyriboles in Lewisian ultramafic rocks. Mineralogical Magazine, 58, 1–20.

Farmer, V.C. (1975) Infra-red spectroscopy in mineral chemistry. In A.W. Nicol, Ed., Physicochemical Methods of Mineral Analysis, p. 357–388. Plenum Press, New York.

Fialips-Guédon, C.-I., Robert, J.-L., and Delbove, F. (2000) Experimental study of Cr incorporation in pargasite. American Mineralogist, 85, 687–693.

Gottschalk, M., Andrut, M., and Melzer, S. (1999) The determination of the cummingtonite content of synthetic tremolite. European Journal of Mineralogy, 11, 967–982.

Hawthorne, F.C. (1997) Short-range order in amphiboles: a bond-valence approach. Canadian Mineralogist, 35, 201–216.

Hawthorne, F.C. and Grundy, H.D. (1976) The crystal chemistry of the amphiboles: IV. X-ray and neutron refinements of the crystal structure of tremolite. Canadian Mineralogist, 14, 334–345.

Hawthorne, F.C., Della Ventura, G., and Robert, J.-L. (1996a) Short-range order and long-range order in amphiboles: A model for the interpretation of infrared spectra in the principal OH-stretching region. In M.D. Dyar, C. McCammon, and M.W. Schaefer, Eds., Mineral spectroscopy, a tribute to Roger G. Burns, Geochemical Society Special Publication 5, p. 49–54.

Hawthorne, F.C., Oberti, R., and Sardone, N. (1996b) Ordering at the A site in clinoamphiboles: the effects of composition on patterns of order. Canadian Mineralogist, 34, 577–593.

Hawthorne, F. C., Della Ventura, G., Robert, J.-L., Welch, M.D., Raudsepp, M., and Jenkins, D.M. (1997) A Rietveld and infrared study of synthetic amphiboles along the potassium-richterite–tremolite join. American Mineralogist, 82, 708–716.

Hawthorne, F.C., Welch, M.D., Della Ventura, G., Liu, S., Robert, J.L., and Jenkins, D.M. (2000) Short-range order in synthetic aluminous tremolites: an infrared and triple-quantum MAS NMR study. American Mineralogist, 85, 1716–1724.

Jenkins, D.M., Sherriff, B. L., Cramer, J., and Xu, Z. (1997) Al, Si, and Mg occupancies in tetrahedrally and octahedrally coordinated sites in synthetic aluminous tremolite. American Mineralogist, 82, 280–290.

Jenkins, D.M, Ishida, K., Liogys, V., and Ghosh, D. (2002) Cation distribution in amphiboles synthesized along the Ga analogue of the tremolite-aluminotschermakite join. Physics and Chemistry of Minerals, 29, 87–97.

Konishi, H., Akai, J., and Kurokawa, K. (1993) Calcic analog of clinojimthompsonite from the Oeyama Ophiolite, Southwest Japan. Journal of the Geological Society of Japan, 99, 679–682.

Maresch, W.V. and Czank, M. (1988) Crystal chemistry, growth kinetics and phase relationships of structurally disordered (Mn^{2+},Mg)-amphiboles. Fortschritte der Mineralogie, 66, 69–121.

Maresch, W.V., Czank, M., and Schreyer, W. (1994) Growth mechanisms, structural defects and composition of synthetic tremolite: what are the effects on macroscopic properties? Contributions to Mineralogy and Petrology, 118, 297–313.

Melzer, S., Gottschalk, M., Andrut, M., and Heinrich, W. (2000) Crystal chemistry of K-richterite-richterite-tremolite solid solutions: a SEM, EMP, XRD, HRTEM, and IR study. European Journal of Mineralogy, 12, 273–291.

Oberti, R., Hawthorne, F.C., Ungaretti, L., and Cannillo, E. (1995) $^{[6]}$Al disorder in amphiboles from mantle peridotites. Canadian Mineralogist, 33, 867–878.

Pawley, A.R., Graham, C.M., and Navrotsky, A. (1993) Tremolite-richterite amphiboles: Synthesis, compositional and structural characterization, and thermochemistry. American Mineralogist, 78, 23–35.

Raudsepp, M., Turnock, A.C., Hawthorne, F.C., Sherriff, B.L., and Hartman, J.S. (1987) Characterization of synthetic pargasitic amphiboles ($NaCa_2Mg_4M^{3+}Si_6Al_2O_{22}(OH,F)_2$; M^{3+}=Al, Cr, Ga, Sc, In) by infrared spectroscopy, Rietveld structure refinement and ^{27}Al, ^{29}Si and ^{19}F MAS nmr spectroscopy. American Mineralogist, 72, 580–593.

Robert, J.-L., Della Ventura, G., Welch, M.D., and Hawthorne, F.C. (2000) The OH-F substitution in synthetic pargasite at 1.5 kbar, 850 °C. American Mineralogist, 85, 926–931.

Sharma, A. and Jenkins, D.M. (1999) Hydrothermal synthesis of amphiboles along the tremolite-pargasite join and in the ternary system tremolite-pargasite-cummingtonite. American Mineralogist, 84, 1304–1318.

Skogby, H. and Rossman, G. (1991) The intensity of amphibole OH bands in the infrared absorption spectrum. Physics and Chemistry of Minerals, 18, 64–68.

Smelik, E.A., Jenkins, D.M., and Navrotsky, A. (1994) A calorimetric study of synthetic amphiboles along the tremolite-tschermakite join and the heats of formation of magnesiohornblende and tschermakite. American Mineralogist, 79, 1110–1122.

Tait, K.T., Hawthorne, F.C., and Della Ventura, G. (2001) Al-Mg disorder in gem-quality pargasite from Baffin Island, Nunavut, Canada. Canadian Mineralogist, 39, 1725–1732.

Veblen, D.R. (1991) Polysomatism and polysomatic series: A review and applications. American Mineralogist, 76, 801–826.

Veblen, D.R. and Buseck, P.R. (1979) Chain-width order and disorder in biopyriboles. American Mineralogist, 64, 687–700.

Welch, M.D. and Knight, K.S. (1999) A neutron powder diffraction study of cation ordering in high-temperature synthetic amphiboles. European Journal of Mineralogy, 11, 321–331.

Welch, M.D., Kolodziejski, W., and Klinowski, J. (1994) A multinuclear NMR study of synthetic pargasite. American Mineralogist, 79, 261–268.

Welch, M.D., Liu, S., and Klinowski, J. (1998) ^{29}Si MAS NMR systematics of calcic and sodic-calcic amphiboles. American Mineralogist, 83, 85–96.

Wood, B.J. and Fraser, D. G. (1976) Elementary Thermodynamics for Geologists, 303 p. Oxford University Press.

Zimmerman, R., Heinrich, W., and Franz, G. (1996) Tremolite synthesis from $CaCl_2$-bearing aqueous solutions. European Journal of Mineralogy, 8, 767–776.

MANUSCRIPT RECEIVED JULY 29, 2002
MANUSCRIPT ACCEPTED FEBRUARY 17, 2003
MANUSCRIPT HANDLED BY LEE GROAT